Soft Matter

Accepted Manuscript

This article can be cited before page numbers have been issued, to do this please use: R. Holyst, M. Litniewski, D. Jakubczyk, M. Zientara and M. Wozniak, *Soft Matter*, 2013, DOI: 10.1039/C3SM50997D.

View Article Online
DOI: 10.1039/C3SM50997D

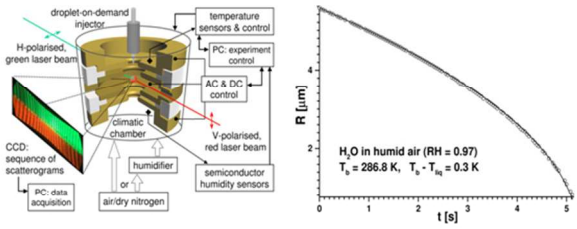

254x190mm (96 x 96 DPI)

View Article Online
ARTICLE TYPE
www.rsc.org/xxxxxx | XXXXXXXX
DOI: 10.1039/C3SM50570X

Nanoscale transport of energy and mass flux during evaporation of liquid droplets into inert gas: computer simulations and experiments

Robert Hołyst[*a], Marek Litniewski[a], Daniel Jakubczyk[b], Marcin Zientara[b], Mariusz Woźniak[b]

Received (in XXX, XXX) Xth XXXXXXXXX 200X, Accepted Xth XXXXXXXXX 200X
First published on the web Xth XXXXXXXXX 200X
DOI: 10.1039/b000000x

We use molecular dynamics (MD) simulations of two component Lennard-Jones (LJ) fluid to analyze the energy flux from an inert gas to the interface of evaporating liquid droplet. Using this analysis we derive an analytical equation for a radius of the droplet, R(t), as a function of time, t. The formula is valid for evaporation of droplets of any material or size into the gas characterized by the mean free path, λ, much larger than the molecular diameter, σ. We find linear dependence R(t)~t, for high λ/R(t) ratio and standard law $R^2(t)$~t for small λ/R(t) ratio. We apply equation for R(t) to experimental results of evaporation of water micro-droplets into air and glycerol, diethylene glycol and triethylene glycol micro-droplets into the nitrogen gas evaporating in time from seconds to tens of minutes. The experimental results together with computer simulations span 12 orders of magnitude of evaporation times and more than 3 orders of magnitude of droplets radii. In the experiments the evaporation rate is governed by very small difference of temperatures (from one tenth of mK to few K) between the gas far from the droplet and evaporating liquid. From MD simulations we obtain also proper boundary conditions for the energy flux at the interface, used in irreversible thermodynamics, and the accommodation coefficients used in kinetic models of evaporation.

Introduction

Evaporation is a process strongly dependent on energy and mass fluxes near interfaces of evaporating liquids[1]. If for any reason the fluxes are impeded the whole dynamical pathway of the process changes[2,3]. For a very long time it has been commonly accepted that the mass and energy(heat) fluxes are reduced at the vapor-liquid interface during evaporation due to some extra barriers not related to the cohesive forces of liquids[3-6]. Two phenonemological coefficients have been introduced to account for the barriers: the thermal accommodation coefficient for the heat flux and the condensation coefficient (probability for vapor molecules to condense upon impinging on the interface) for the mass flux[3].

Varilly and Chandler showed[7] in computer simulations that water molecule had probability near unity to condense upon impinging on the surface of water. These simulations excluded a possibility of existence of any additional barrier for the mass flux and set the condensation coefficient at the value equaled to 1. But the problem of additional barriers for a heat transfer from vapor to liquid during evaporation remained open. The experiments of Ward and coworkers[8-11] showed a temperature discontinuity at the water-vapor interface during evaporation of water at low vapour pressures. This discontinuity was also determined in computer simulations for the one-component Lennard-Jones fluid[12]. Such discontinuity indicated that the transport of heat was in some way impeded during evaporation. Reduction of the heat transport during evaporation could explain the results of Saykally and coworkers[5] who obtained smaller than unity condensation coefficient on the basis of temperature measurements inside evaporating droplets.

Any discontinuity in temperature profile needs proper boundary conditions in order to apply irreversible thermodynamics and a direct relation of the heat flux to the temperature gradients near the interface[13]. The kinetic theory alone cannot simply be used to determine the heat flux in the system, but can be used to formulate the proper boundary conditions[1]. Although there is no apparent barrier for the mass flux as shown by Varilly and Chandler[7], a reduction of the heat flux would have similar effect as the barrier i.e. the mass flux would be reduced.

We address a number of questions in this paper: what is the energy flux from the vapor to the liquid during evaporation of liquid droplets? Under which thermodynamic conditions this flux is reduced near the interface? What is the analytical formula for the mass flux, applicable to a wide range of experimental systems? What is the thermal accommodation coefficient?

We performed computer simulations of the two-component Lennard-Jones system and analyzed the temperature gradients and the heat transfer from hot vapor to the interface of evaporating droplet. We analyzed these quantities as a function of the droplet Knudsen number (ratio of the mean free path, λ, of molecules in the vapour to the radius of evaporating droplet)[14]. One of the components constituted an inert gas and the second component formed a liquid droplet. The temperature of evaporation was set between the critical temperatures of these two components i.e. the gas component was well above its critical point and the liquid component was well below its proper critical point. The obtained results were tested against experimental results for evaporation of water into air, and glycerol, diethylene glycol, and triethylene glycol into dry nitrogen atmosphere.

View Article Online
DOI: 10.1039/C3SM50997D

The paper is organized as follows: In the next two sections we give details of computer simulations and experimental set-up. Next we discuss the temperature profiles and the mass flux arising from the energy flux. We compare theory with experiment, discuss the accommodation coefficient and conclude the paper with the summary of obtained results.

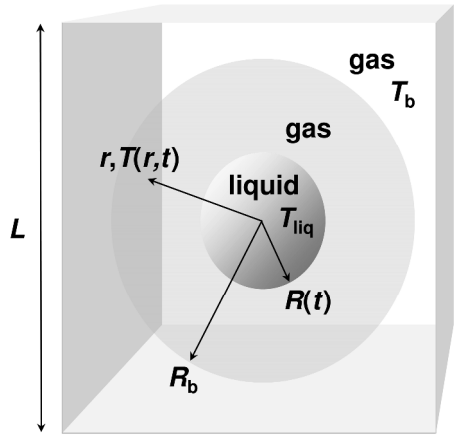

Fig.1 A schematic picture of the system during simulation run. The gas temperature was fixed at T_b for $r>R_b$ (by scaling velocities of particles), The size of the system L was changed between 340 and 990 (in the units of the molecular diameter σ) and R_b was approximately equal to L/2 (see the Supporting Information). The radius of the droplet R(t=0) was between 24 and 36. The liquid droplet had constant temperature during evaporation, T_{liq} smaller than T_b . After short initial transient state(see Fig.S2 in Supporting Information), the temperature profile T(r,t) was quasi-stationary i.e. it quickly adapted to the changes of the droplet radius R(t) in time, t, i.e. T(r,t)=T(r/R(t)) during the quasi-stationary regime of evaporation.

Details of computer simulations

We used the classical constant NVE molecular dynamics method (MD)[15] in two-component system. The particles interacted via the truncated and shifted Lennard-Jones (LJ) potential in the following form:

$$u_{ij} = 4\varepsilon_{ij}\left(\left(\frac{\sigma_{ij}}{r}\right)^{12} - \left(\frac{\sigma_{ij}}{r}\right)^{6}\right) - 4\varepsilon_{ij}\left(\left(\frac{\sigma_{ij}}{d}\right)^{12} - \left(\frac{\sigma_{ij}}{d}\right)^{6}\right) \quad (1)$$

for $r<d=2.5\ \sigma_{ij}$ (ij – indices for each component) and 0 otherwise. All particles had the same mass m and size σ (i.e. the size parameters $\sigma_{11} = \sigma_{12} = \sigma_{22} \equiv \sigma$) and differed only by the energy parameters for which the ratio $\eta = \varepsilon_{22}/\varepsilon_{11} \le 0.5$. The mixing rule was $\varepsilon_{12} = \varepsilon_{22}$. The Newton equations of motion were solved using the Verlet "leapfrog" scheme[15,16] with the time step $\delta t = 0.01\ \sigma_{11}(m/\varepsilon_{11})^{1/2}$. All numerical values presented further were expressed in the reduced units of the first component (i.e. $\sigma = \varepsilon_{11} = m = 1.0$). The temperature was always given in ε_{11}/k_B where k_B is the Boltzmann constant. Particles of the first component formed a droplet of the radius R of the number liquid density ρ_{liq} and the liquid temperature T_{liq}. The liquid droplet of the first component was immersed in the center of the system and evaporated into the inert gas composed of the particles of the second component. The droplet radius R was defined via the total number density i.e. $\rho(r=R)=\rho_{liq}/2$. The total number of particles used in the simulations were from 2.6×10^6 to 7×10^6. The ratio of the number of particles of the component 1 to the particles of the component 2 was never higher than 0.036. A schematic picture of the system was shown in Fig. 1. The liquid made of the first component was at the thermodynamic conditions well below its proper critical point. For Eq.(1) the critical temperature for this substance was found equal to[17] 1.08 while the second component forming an inert gas was well above its critical point. Such situation corresponded to the experimental case of evaporation of liquids (e.g. water) into the inert gas e.g. air.

Simulations of the evaporation process were performed in a cubic box of size L with periodic boundary conditions (Fig.1). The initial conditions for each simulation run were taken from additional simulations for the system composed of the first component particles, only. In these simulations the liquid droplet of the radius $R(0)$ was at equilibrium with the surrounding gas (typical parameters were shown in the Table S1 of the Supporting Information). At the very beginning of the run (t=0) all particles at distance r such that $\rho(r)<0.25$ were converted into the second component particles. The conversion led to decrease of the gas temperature because ε_{11} differed from ε_{22}. In order to make the initial equilibrium temperature of the gas equaled to that of the droplet some heat was added at t = 0 by scaling the velocities of the gas particles. Added heat was determined from additional simulations for a pure gas phase. During the whole evaporation process the temperature of the gas at the distance $r>R_b$ from the center of the droplet was kept constant $T=T_b$ by scaling the velocities. Because of the periodic boundary condition the first component particles could come back, after evaporation, to the droplet and obstruct the evaporation process. Such return of particles via boundaries was unphysical, because it was driven purely by the boundary conditions in the simulation box and not by molecular collisions. Therefore all the first component particles that crossed the box border and came back at r lower than R_{el} (see Table S1 in the Supporting information) were removed from the system.. We checked that, the influence of R_{el} on the time evolutions considered here was completely negligible.

The simulations of evaporation process were performed for six values of T_b from 0.711 to 0.948 and $\eta = 0.5$. For $T_b = 0.903$ the ratios of the energy parameters $\eta = 0.05$, 0.005 and 0.0005 were also considered. The central part of the droplet was nearly non-attainable for the second component and the fraction of the first component into the gas was very low (see Figure S1 and Table S2 in Supporting information).

Detail of experimental set-up

Electro-dynamic trapping, used here to levitate single droplets, is a well-established experimental technique[6,18-24]. A particular combination of alternating (AC) and static (DC) electric fields, in (close to) quadrupolar configuration, enables constraining particle to a small volume of "free" space, ideally to a point. Particle of a certain charge to mass ratio sit then in the pseudo-potential

View Article Online
DOI: 10.1039/C3SM50997D

minimum formed by oscillating quadrupolar field. We use two traps of slightly different design, both built in our lab. Both traps

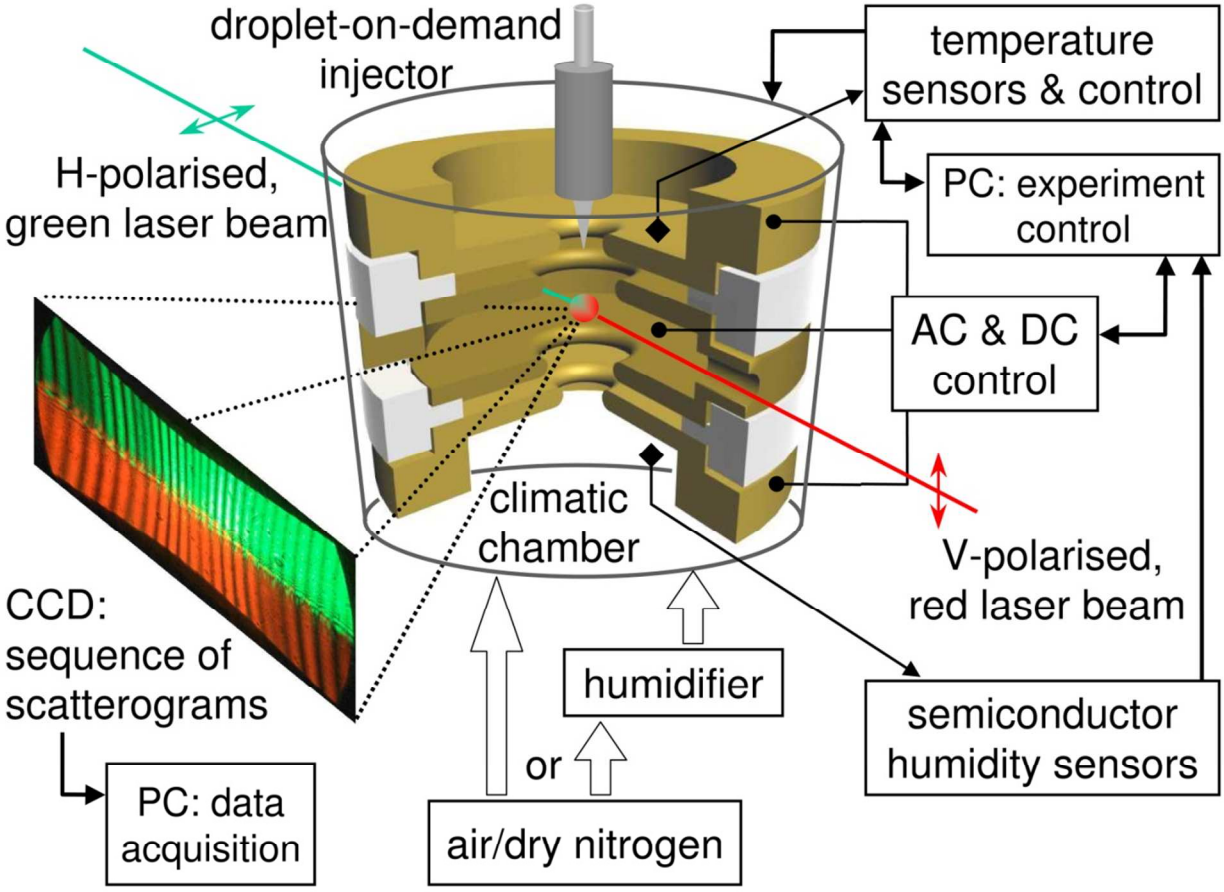

Fig.2 Schematic drawing of experimental setup. Cutaway drawing of the electrodynamic quadrupole trap together with the droplet-on-demand injector shown in the centre. Droplet presented as ~100× oversized. Semiconductor humidity sensors give tentative relative humidity value. DC control was also used for droplet positioning.

are kept in small (~10 cm^3) thermostatic chambers at atmospheric pressure. One of the chambers was Peltier-element-ooled and can be filled with the mixture of nitrogen/air and (nearly) saturated water vapour. Another is electrically heated and can be filled with dry nitrogen. They are used for experiment with water and glycols respectively. The experimental setup is shown schematically in Fig.2.

The droplets were injected into the trap with the piezo-type, droplet-on-demand injectors (several designs[25] were built and tested in our lab) kept at chamber temperature. The droplets were charged by charge separation in the external field of the trap, on emerging from the injector nozzle (no additional charging electrodes were used). Thus, the sign and the value of the charge was, to some extent, determined by the injection timing versus the phase of the trapping AC field. Our setup allowed stable trapping of droplets of radii from ~35 down to ~0.5 μm. The average initial droplet radius was several μm. No secular (macro) motion was allowed or observed.

Two coaxial, counter propagating laser beams were used simultaneously for droplet illumination: green (532 nm, ~5.5 mW) H-polarised (horizontal) and red (633 nm or 654 nm, ~10 mW) V-polarised (vertical). Neither photophoresis nor thermophoresis nor radiation pressure effects were observed. Two linear polarisers were used in the detection channel: H-polariser (in respect to the scattering plane; upper half of the channel) and the V-polariser (the lower half of the channel). The distortions of spatial frequency and shape of the interference fringes (spherical aberration and other geometrical effects) were corrected numerically in post-processing. Entirely defocused images of the droplet (scatterograms) were registered with a colour CCD camera (PixelFly, pco.imaging), at the right angle to the laser beams in the horizontal scattering plane.

The temporal evolution of the droplet radius R(t) was obtained by analysing the recorded scatterograms (angle-resolved static light scattering). The total error of R is of the order of several nm, while the error of time t is smaller than 10 ms. The angular distribution of scattered light intensity was analysed within the framework of the Mie theory for every acquired scatterogram. This well established interferometric technique was used for particle characterisation[26] (and references therein). Its variants (laser imaging for droplet sizing (ILIDS), interferometric particle imaging (IPI), Mie scattering imaging (MSI), interferometric Mie imaging (IMI), etc.) were used for particle sizing e.g. in sprays. The variant of our method belonged to a

View Article Online
DOI: 10.1039/C3SM50997D

group of look-up table methods based on comparing experimentally obtained versus theoretically predicted scattering patterns[6,27] (for experiments with water and with slowly evaporating liquids).

In the presented experiments we used: diethylene glycol (DEG; BioUltra, 99.99 GC%, Fluka), triethylene glycol (TEG; BioUltra, anhydrous, 99.96 GC%, Fluka) and ultra pure water (~18 MΩcm, total dissolved solids <20 ppb, produced in the lab with Milli-Q Plus, Millipore). Liquids were quickly transferred into the droplet injector with a sterile syringe and the experiments were conducted within 1 hour after injector loading. The changes of resistivity of ultra pure water loaded into the injector placed in ambient air were carefully measured in the separate experiment. It was estimated that during the first hour after purification the total dissolved solids concentration would grow to ~60 ppb, which was still satisfactory. The results published for sodium dodecyl sulphate (SDS) in water[21] and our results for SDS in DEG seemed to indicate that the surface activity of impurities had no significant additional influence upon evaporation. Refractive indices and densities of glycols used in experiments were provided by the manufacturers of the chemicals. The dispersion curves for DEG and TEG were adapted from other work[28]. All thermodynamic data for gaseous nitrogen and air (heat capacity and heat conductivity) were taken from Ref(29). We used previous data for evaporation of water, diethylene glycol, triethylene glycol (evaporation times were between seconds and tens of seconds) and added new experiments on evaporation of glycerol (evaporation time was almost 40 minutes).

Estimation of the mean free path

The temperature discontinuity found by Ward and coworkers occurred for low water vapour pressure and therefore high mean free path, λ, of water molecules in the vapour[9-11]. The computer simulations and solutions of the equation of irreversible thermodynamics[12,13] showed that for small λ (high density of the vapour) the temperature profile is continuous at the liquid-vapour interface. Therefore we expected that λ should play important role in the energy transfer at the interface.

λ is well determined only for hard body systems. For the system of identical spheres that fulfills the Maxwell-Boltzmann distribution λ is the mean distance between collisions [30]:

$$\lambda = \frac{1}{\sqrt{2}\pi\varrho a^2} \qquad (2)$$

where a is the hard body diameter and ρ is the vapour density. We use this formula to estimate λ in our experimental systems. But the above formula cannot be simply transferred to the Lennard-Jones system. The rough approximation $a \approx \sigma$ may be valid only for very rare gas (i.e. $\rho^{-1/3} >> \sigma$) at moderate temperatures. On the other hand, λ is also physically interpreted as a parameter that characterizes the relaxation scale. The scale is directly correlated with the self-diffusion constant D that for the hard body dilute gas can be evaluated as follows[30] :

$$D = \frac{3\sqrt{k_B T/m\pi}}{8\rho a^2} \qquad (3)$$

Eqs. (2) and (3) give the relation

$$\lambda = \frac{8D}{3\sqrt{2\pi k_B T/m}} \qquad (4)$$

The above formula is strictly valid only for the hard body dilute gas however, following the physical interpretation of λ, Eq. (4) can be generalized to gas composed of the LJ particles.

The relation (4) was especially suitable for our purposes. The self-diffusion constants D for particles of the second component in the inert gas at ρ_b and T_b were determined from the Einstein formula by performing additional MD simulations for pure gas[15]. The values of D were used to estimate the mean free path λ according to Eq(4) (see Table S2 in Supporting Information). The estimated λ from the computer simulations ranged from 2 to 20 (in units of the diameter σ). In the experiments the estimated[31] λ was 63 nm for nitrogen at 25 degrees C and 66 nm for humid air at 13 degrees C studied in this paper. Thus these mean free paths were two orders of magnitude larger than water or nitrogen diameter.

Temperature profile and energy flux from computer simulations

The evaporation process observed in simulations could be divided into two stages. During the first stage of evaporation the initial strongly non-equilibrium process was characterized by the sharp decrease of R, rapid decrease of T_{liq} (Fig. S2) and increase of ρ_{liq}. During this stage the droplet evaporated at the expense of its own internal energy, because at the beginning of the process the temperature of the liquid was equal to the temperature of the vapour. This stage lasted for a short time. Much longer was the second quasi-stationary stage, described in detail below. Important remark: we had no control over the final temperature T_{liq} and we could not predict this temperature apriori before performing the computer simulations. A longer discussion of this problem was given by us in the summary section.

We observed that the temperature profiles quickly adjusted to the changes of the radius of the droplet $R(t)$. The profiles were quasi-stationary i.e. $T(r,t)=T(r/R(t))$. Additionally the temperature of the droplet T_{liq} was nearly constant during evaporation (except for very small droplets) (see Fig.S2 in Supporting Information). Our previous simulations[12] showed that far from the droplet the temperature profile obeyed the following equation:

$$\frac{1}{r^2}\frac{\partial}{\partial r}\left(r^2 \kappa_v \frac{\partial T}{\partial r}\right) = 0 \qquad (5)$$

κ_v was the heat conductivity in the vapour phase composed of the of the second component. The terms related to the mass transport i.e. radial velocity u could be neglected[13]. According to Eq. (5) the heat flux for the process $j_h(r)$ far from the droplet interface fulfilled the following relations:

$$r^2 j_h(r) = R_b^2 j_h(R_b) = -R_b^2 \kappa_v \frac{\partial T}{\partial r}\Big|_{r=R_b} \qquad (6)$$

where R_b was the boundary shown in Fig. 1. The above equation was more general than (5). Eq. (6) was correct even in vicinity of

View Article Online
DOI: 10.1039/C3SM50997D

the interface and allowed to define proper boundary conditions at the interface used in irreversible thermodynamics. Moreover since the liquid temperature was constant during evaporation Eq(6) was used here to predict the energy flux at the interface. Neglecting non-uniformity of κ_v, the solution of (5) was determined by R_b, T_b, and $j_h(R_b)$:

$$T(r,t) = \frac{\left(R_b T_b - R(t) T_X - R_b R(t)\frac{(T_b - T_X)}{r}\right)}{(R_b - R(t))} \qquad (7)$$

where T_X was obtained from extrapolation of Eq(6) to the interface at $r=R(t)$ (dashed line in Fig.3) and followed from the temperature gradient at the boundary layer located at $r=R_b$ (see Fig.1) :

$$\left.\frac{\partial T}{\partial r}\right|_{r=R_b} = \frac{R(t)(T_b - T_X)}{R_b(R_b - R(t))} \qquad (8)$$

The left hand side of (8) was determined at any point along the temperature profile, where Eq(5) applied, and used to calculate the extrapolation temperature. In practice, we determined T_X directly from the data by fitting part of the $T(r, t)$ profile taken from the simulation to Eq. (7). This part had to be chosen at a certain distance from the interface, because Eq(5) was not correct close to the interface where abrupt changes of temperature were measured[8-11] and determined in simulations[12]. The data coming from this region were discarded in the fit. Thus we made a fit of the function given by Eq(7) in the region $R_b \geq r \geq R_{fit}$. The choice of R_{fit} was based on the observation of the evaporation process. For $R_{fit} > R(t)+3\lambda$, T_X did not depend on R_{fit}.

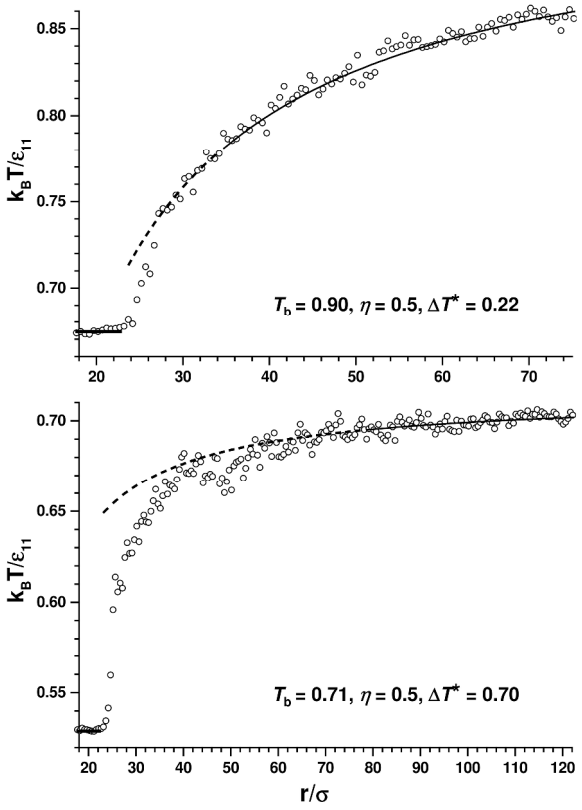

Fig.3 Temperature profiles for quasi-stationary stage of evaporation for two simulation systems. The empty circles are simulation results. The solid line (continued as a dashed line for extrapolation) is the theoretical result from Eq(7) with T_X being a free fitting parameter (see also Eq. (9,10) for the definition of ΔT^*). T_X is the result of extrapolation of the temperature profile far from the interface down to the interfacial region, thus ΔT^* is the discontinuity of the temperature at the interface i.e. at r=R(t). We always get non-zero value of ΔT^* even for $T_b = 0.903$, where previously for the one component system LJ we got smooth temperature variation[12]. In our previous paper[12] , however, small temperature differences were not recognized properly due to the fitting procedure.

We divided the whole evaporation process into 30 – 50 equal time intervals sufficiently short that the changes in $R(t)$ and in the local thermodynamic parameters of the system during the second stage of the process could be neglected. For each of the intervals, $T(r, t)$ was fitted to (7) using the least square method for $r \geq R_{fit}$. The values of T_X obtained from the procedure were used to calculate the temperature difference ΔT between the extrapolated temperature obtained from Eq(5) and the actual temperature of the liquid droplet:

$$\Delta T = T_X - T_{liq} \qquad (9)$$

We found ΔT to be always positive. Differently to the previous paper[12] ΔT obtained in this way was a measure of the deviation of the temperature profile from the hydrodynamic model and also could be used as a definition of a real discontinuity at the interface (see Fig. 3). Analyzing the dependence of ΔT on R(t) and λ we found that the relative value:

$$\Delta T^* = \frac{\Delta T}{(T_b - T_{liq})} \qquad (10)$$

can be approximated by:

$$\Delta T^* \approx f\left(\frac{R(t)}{\lambda}\right) = \frac{1}{1 + R(t)/(A\lambda)} \qquad (11)$$

where A is a constant for a given system with fixed λ.We fitted ΔT^* to $f(R/\lambda)$ by using the least square method. ΔT^* as a function

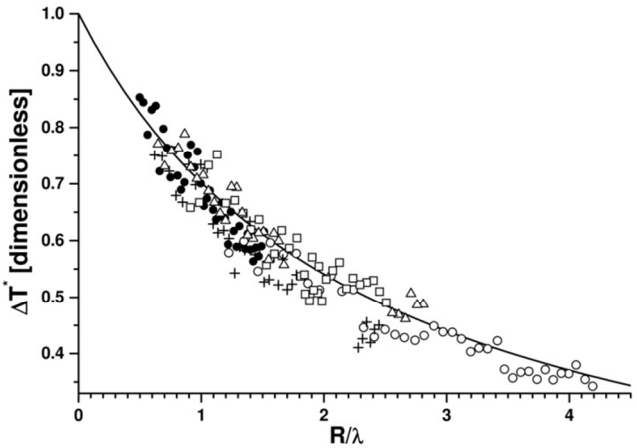

Fig.4 Solid line: $f_A(R/\lambda)$ given by Eq(11) for $A = 2.35$. In all these cases the mean free path was much larger than the molecular diameter ($\lambda >> \sigma$) and/or interaction between molecules were negligible i.e. $\eta << 1$. Symbols: crosses ($T_b = 0.75$, $\eta = 0.5$), solid circles ($T_b = 0.71$, $\eta = 0.5$), open squares ($T_b = 0.9$, $\eta = 0.005$), open circles ($T_b = 0.90$, $\eta = 0.05$), open triangles ($T_b = 0.9$, $\eta = 0.0005$). In all these cases the vapour could

View Article Online
DOI: 10.1039/C3SM50997D

be approximated by the ideal gas. For the value of A for other systems with small mean free path see Table S2 in the Supplementary Information.

of R/λ for all simulations is shown in Fig. 4. We found that for large $\lambda >> \sigma$ (i.e. for a very dilute vapor) the parameter A approached a constant value 2.2-2.4 independent from any thermodynamic or kinetic variables. Such conditions characterized our experiments for evaporation of droplets into air, or nitrogen where λ=66 nm was more than two orders of magnitude larger than σ. The values of A for dense vapor also obtained from the simulations were presented in Table S2 in the Supporting Information. When the vapor density increased A approached 0.

The extrapolated temperature T_X was used to calculate the energy flux at the droplet-vapour interface (see Eq.(7)). For $R_b >> R(t)$ we got from Eq.(7) and Eq. (9-11):

$$j_h(r,t) = -\kappa_v \frac{\partial T}{\partial r}\Big|_{r=R(t)} = -\kappa_v \frac{(T_b - T_X)}{R(t)} = -\kappa_v \frac{(T_b - T_{liq})}{A\lambda + R(t)} \quad (12)$$

The minus sign reflects the direction of the energy flux opposite to the normal to the surface. The flux was obtained on the basis of irreversible thermodynamics[12,13] with proper boundary conditions determined here by molecular simulations. In the supporting information we showed that the conductivity, κ_v, did not change appreciably in the vapour phase[32].

The mass flux from the energy flux during evaporation of a droplet

Because the liquid evaporated at constant temperature the whole energy flux was consumed by the mass flux leaving the droplet surface. From the conservation of energy we got the following equation relating the change of the droplet radius to the energy flux:

$$\Delta h \varrho_{liq} \frac{\partial R(t)}{\partial t} = -\kappa_v \frac{(T_b - T_{liq})}{A\lambda + R(t)} \quad (13)$$

where $\Delta h = h(T_b) - h(T_{liq})$ was the total change of the enthalpy per unit mass upon evaporation. ρ_{liq} was the liquid density. These parameters were independently determined in separate simulations. The values of κ_v were determined from additional MD simulation using the method of Muller-Plathe[32]. Figure 5 showed dR/dt evaluated from (13) and directly from computer simulations. All parameters in Eq(13) were determined in independent simulations therefore the comparison shown in Fig.5 did not contain any adjustable parameters. However T_{liq}, which established after the initial transient non-stationary regime of evaporation, could not be predicted apriori (Fig. S2), but only aposteriori (see also summary section)

Two limits emerged[14] from Eq(13). When $A\lambda >> R(t)$ (large droplet Knudsen number) the droplet radius, R(t), changed linearly with time, t, while in the opposite limit of small droplet Knudsen number $R^2(t)$ changed linearly with t.

Experimental results for radius of evaporating droplet as a function of time

In this section we discussed evaporation of four different experimental systems (glycerol, diethylene glycol, triethylene glycol evaporating into the nitrogen and water evaporating into air). We compared the results to Eq(13) predicted on the basis of computer simulations of two component Lennard-Jones fluid. In all fits we fixed A=2.35 since in all cases the inert gas was characterized by very large mean free path, much larger than the molecular diameter.

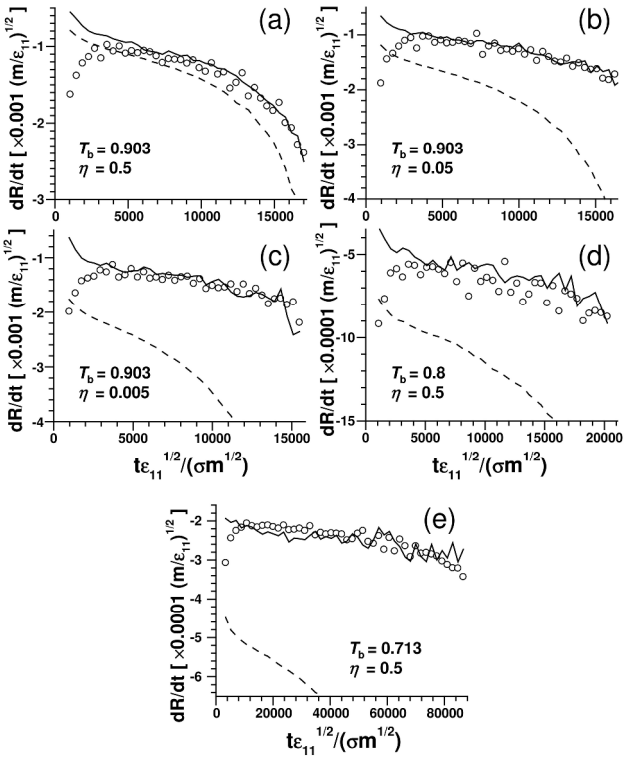

Fig.5 dR/dt determined from the simulations (filled circles) and from Eq. (13) (the solid line). The dashed line is for the model with $\Delta T^* \equiv 0$. ΔT^* was determined from Eq(7) by fitting the temperature profile to the simulation data. The deviations for short times come from initial strongly non-equilibrium stage of the evaporation. The fit in all these simulations did not contain any free parameters: Δh , ρ_{liq}, κ_v were determined from independent computer simulations (see e.g. supporting information).

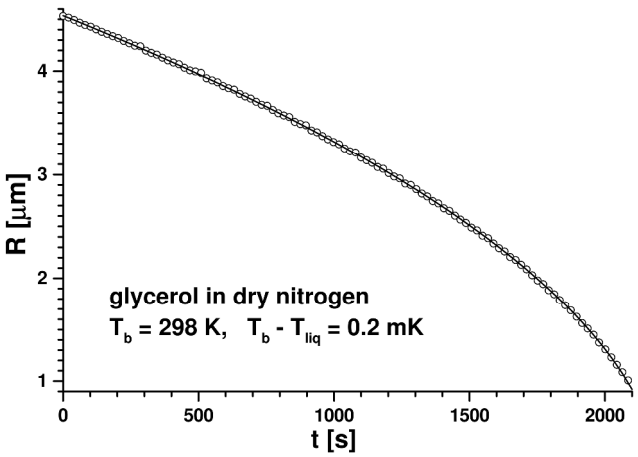

Fig.6 The radius of the glycerol droplet as a function of time during evaporation into the dry nitrogen vapour (solid line is the theory resulting

View Article Online
DOI: 10.1039/C3SM50997D

from integrating Eq.(13) and solid circles are the experimental results). The following parameters characterized the system: Δh= 996 kJ/kg ,ρ_{liq}= 1257 kg/m^3, κ_v=0.0258 J/m·s·K, λ=66 nm. The value of A was set at 2.35 as determined in computer simulations for the two component LJ system (see Fig.4). The only free parameter in the fit was the temperature difference between the vapour temperature far from the droplet T_b and the droplet temperature T_{liq}. Very small temperature difference leads to very small evaporation rates (see also comparative results for all substances shown in Fig.7).

An example of the fit for evaporation of glycerol was shown in Fig.6. The single fitting parameter was the temperature difference between gas far from the droplet, T_b, and droplet of glycerol, T_{liq}.

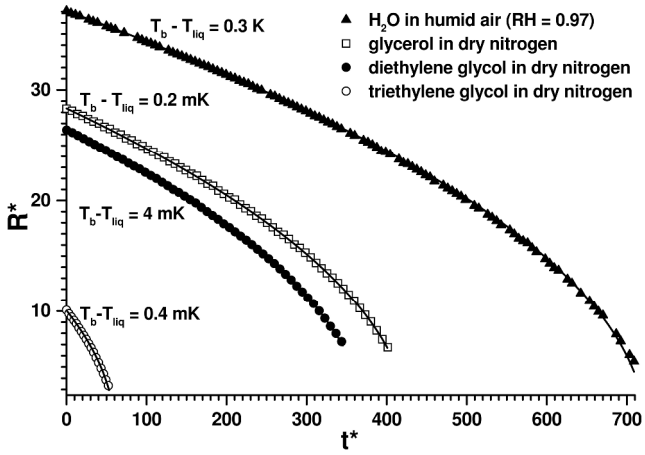

Fig.7 The dimensionless radius of droplets $R^*=R(t)/(A\lambda)$ for four different liquids (water, glycerol, diethylene glycol and triethylene glycol) is shown as a function of dimensionless time $t^*=t/\tau$ where $\tau=(A\lambda)^2\Delta h\rho_{liq}/(\kappa_v(T_b-T_{liq})$ is the characteristic time for evaporation. This rescaling makes Eq(13) universal i.e. free from any material parameters. The characteristic time, τ, is as follows: τ=7.2 ms for water, τ=0.14 s for diethylene glycol, τ=1.4 s for triethylene glycol and τ=5.2 s for glycerol. This time gives the total time of evaporation for a droplet of radius $A\lambda$ for the temperature difference T_b-T_{liq}. The initial size of the droplets in our experiments is R(t=0)=4.2 μm for diethylene glycol; R(t=0)=5.6 μm for water and R(t=0)=1.6 μm for triethylene glycol. The solid lines result from integrating Eq(13) and symbols are the experimental results. The experimental errors are smaller than the symbols. The thermal conductivity and the mean free path of dry nitrogen at 298 K were κ_v=0.0258 J/m·s·K and λ=66 nm respectively, while for humid air (RH=0.97) at 286 K they were κ_v=0.0248 J/m·s·K and λ=63 nm respectively. The following parameters characterized the liquids: (for glycerol see Fig.6); for triethylene glycol Δh=527 kJ/kg ,ρ_{liq}=1121 kg/m^3; for diethylene glycol Δh=546 kJ/kg ,ρ_{liq}=1114 kg/m^3 and for water Δh=2442 kJ/kg ,ρ_{liq}=997 kg/m^3 . The value of A was set at 2.35 as determined in computer simulations (see Fig.4). The only free parameter in the fit was the temperature difference between the vapour temperature far from the droplet T_b and the droplet temperature T_{liq}. In computer simulations the difference is known, but we don't have a method for predicting T_{liq} apriori before actually performing the experiment or computer simulations (see also Fig.S2 and summary section).

In case of rather noisy data, we found it advantageous to integrate equation (13) first and fit the integrated form to unprocessed data rather than to calculate the time derivative of the experimental data and directly fit (13). The solid curve in figures 6,7 demonstrated such fit for four different substances. The evaporation rate changed by 3 orders of magnitude and the radii changed by almost an order of magnitude. The quality of the fit with a single parameter (the temperature difference T_b-T_{liq}) was remarkably good for all cases. These comparisons gave, together with results from computer simulations (comparison between simulation and Eq(13) at Fig. 5 without any free parameter), a very strong support for the theoretical model summarized by Eq(13). From equation (13) it followed that the magnitude of the sought effect was controlled by $A\lambda/R$. The kinetic effects manifest only when $A\lambda/R$ was larger than the experimental uncertainties. In case of our experiments under atmospheric pressure ($\lambda\approx$70 nm) such condition required $R\approx<1$ μm. The influence of ubiquitous impurities could mask the sought effect to some extent. We demonstrated[1,33] that even if no apparent effects of impurities were visible, their influence upon the retrieved thermodynamic quantities might reach several percent. It could lead to overestimation of coefficient A. The effect of impurities was minimized by utilizing high-purity samples. Since the concentration of (non-volatile) impurities increased as the droplet evaporated, the cases in which the droplet radius changed significantly should be excluded. Here we presented four examples of small droplets of liquids of different volatility, complying with postulated constraints. The considered effect was observed regardless of the temporal span of evolution.

Eq.(13) enabled determination of T_b-T_{liq}. T_{liq} was not measured independently in the experiments, as we did in the computer simulations. Since T_b could be determined with good accuracy, the temperature of the droplet could be retrieved in this way with unparalleled accuracy, not easily achieved by other methods based on temperature dependence of fluorescence spectra[5].

The thermal accommodation coefficient

The parameter A was related to the thermal accommodation coefficient[1,34] α_T and also the condensation coefficient α_C. The parameter A was expressed in two equivalent forms[1]:

$$A=\frac{\kappa_v\sqrt{2\pi M/(RT_{liq})}}{\lambda\rho_v c_p\alpha_T} \quad (14)$$

or

$$A=\frac{D\sqrt{2\pi M_{liq}/(RT_{liq})}}{\lambda\alpha_C} \quad (15)$$

Here ρ_v was the vapour density, M was the molecular mass of the vapor molecules, M_{liq} was the molecular mass of the molecules from the liquid phase, R was the gas constant and c_p wass the heat capacity of the vapour phase. From Eq(14) and Eq(15) it followed that both coefficients were related by the following equation:

$$\frac{D}{\alpha_C}=\frac{\kappa_v}{\rho_v c_p\alpha_T}\sqrt{\frac{M}{M_{liq}}} \quad (16)$$

Therefore

$$\frac{\alpha_T}{\alpha_C}=\frac{\kappa_v}{\rho_v c_p D}\sqrt{\frac{M}{M_{liq}}}=Le\sqrt{\frac{M}{M_{liq}}} \quad (17)$$

View Article Online
DOI: 10.1039/C3SM50997D

where Le was the Lewis number (see Table S4 in SI). For the approximations given by Eq(3,4) and Eq(15) we found that for LJ system studied by computer simulations (A=2.35) :

$$\alpha_C = \frac{3\pi}{4A} \approx 1 \qquad (18)$$

in accordance with recent results of Varilly and Chandler[7]. The Lewis number Le for the ideal gas was equal to 5/4 and from Eq(17) we found the thermal accommodation coefficent α_T =1.25. For water evaporating into humid air we obtained α_C=1.08, Le=0.87 and α_T=1.2. For glycerol, diethylene glycol and triethylene glycol we got Le~2.4 to 3.7 , α_C~0.74 to 0.9 and α_T~1.2 for all the systems. In general neither α_C nor α_T could be straighforwardly interpreted in terms of probabilities. The *A* parameter could be changed by 20% without visible changes of the quality of the fit to experimental data and therefore the error for the coefficients here is also around 20%. Another issue is the dependence of *A* on molecular masses – in current simulations we set the masses of both components the same. Finally, for LJ liquid evaporating directly into vacuum at constant temperature the mass flux was given by the Hertz-Knudsen (HK) equation[35] multiplied by the evaporation coefficient of value 2 instead of 1.

Conclusions

Equation (13) with A=2.35 together with comparison to experiments shown in Fig.6 summarizes the main result of this publication. This equation is valid for droplet of any material and size evaporating into inert gas, providing that the mean free path in the gas is much larger than molecular diameter. Eq(13) works remarkably well at the scale of micrometers and thousands of seconds (Fig.6) and also at the nanoscale characterized by the droplet size of tens of nm and time scales of the order of tens of nanoseconds (Fig.5). This equation contains one parameter, used to fit experimental data. This is the constant temperature, T_{liq}, of the liquid droplet during evaporation in the quasi-stationary regime. Before reaching the regime the droplet of the initial temperature, T_b, same as the temperature of the gas evaporates mostly at the expense of its internal energy (see FigS2 in SI). Thus initially (in a very short period of time) the droplet temperature decreases. The decrease of the temperature stops at a certain value equal to T_{liq}. For this temperature the energy flux from the gas matches the enthalphy of evaporation multiplied by the mass flux. In principle T_{liq} is easily determined in computer simulations and can be measured, in principle, in experiments. But for a given thermodynamic state of the gas and a given evaporating substances with known equilibrium partial pressure we should be able to predict T_{liq} apriori, before actually performing the experiment or running the computer simulations. Predicting T_{liq} apriori requires additional relation for the mass flux independent from Eq(13). An example of such independent relation for the mass flux is the Hertz-Knudsen (HK) equation[36]. Two different equations (Eq(13) and HK equation) must give the same mass flux. Thus T_{liq} can be predicted apriori from this additional equality. Before proper HK equation is formulated two problems have to be resolved: what is the temperature which we should use in the estimation of the saturation pressure in the Hertz-Knudsen equation? How should we account for the change of partial pressure of evaporating substance near the interface?

Acknowledgement: This work was supported by the Ministry of Science and Higher Education/European Science Foundation (ESF/PESC EPSD program) as a scientific project 2010–2013.

Notes and references

[a] *Institute of Physical Chemistry Polish Academy of Sciences, Kasprzaka 44/52,01-224 Warsaw,Poland* rholyst@ichf.edu.pl mlitniewski@ichf.edu.pl
[b] *Institute of Physics of the Polish Academy of Sciences,Al Lotnikow 32-46, PL-02668 , Warsaw, Poland*

† Electronic Supplementary Information (ESI) available: [details of MD simulations]. See DOI: 10.1039/b000000x/

1 R. Hołyst, M. Litniewski, D. Jakubczyk, K. Kolwas, M. Kolwas, K. Kowalski, S. Migacz, S. Palesa and M. Zientara *Rep.Prog.Phys.* 2013, **76**, 034601.
2 R.Hołyst, *Pure Appl. Chem.*2009, **81**, 1719.
3 R.A.Shaw and D.Lamb, *J.Chem.Phys.* 1999, **111**, 10659.
4 N.A. Fuchs, *Evaporation and droplet growth in gaseous media*, Pergamon 1959.
5 J.D.Smith, C.D.Cappa, W.S.Drisdell, R.C.Cohen, R.J.Saykally, *J.Am.Chem.Soc.*2006, **128**, 12892.
6 D.Jakubczyk, G.Derkachov, T.Do-Duc, K.Kolwas, M.Kolwas, *J.Phys.Chem. A* 2010, **114**, 3483.
7 P.Varilly and D.Chandler, J.Phys.Chem. B 2013, **117**, 1419.
8 G.Fang and C.A.Ward, *Phys.Rev.E* 1999, **59**, 417.
9 C.A.Ward and G.Fang, *Phys.Rev. E* 1999, **59**, 429.
10 G.Fang and C.A.Ward, *Phys.Rev. E* 1999, **59**, 441.
11 AJH. MacGaughey and C.A.Ward, *J.Appl.Phys.* 2002, **91**, 6406.
12 R.Hołyst and M.Litniewski, *Phys.Rev.Lett.* 2008, **100**, 055701.
13 V.Babin and R.Hołyst, *J.Phys.Chem. B*, 2005, **109**, 11367.
14 E.S.Laundry, S.Mikkilineni, M.Paharia and A.J.H.Macgaughey *J.Appl.Phys*. 2007, **102**, 124301.
15 M.P. Allen and D. Tildesley, *Computer Simulations of Liquids* 1987 (Oxford University Press)
16 L. Verlet, *Phys. Rev*. 1967, **159**, 98.
17 J. Vrabec, G. K. Kedia,G. Fuchs and H. Hasse, Mol. Phys. 2006, **104**, 1509.
18 F.G. Major, V.N. Gheorghe and G. Werth G 2005 *Charged Particle Traps* (Berlin: Springer).
19 W.Paul *Rev.Mod.Phys*. 1990, **62**, 531.
20 S.Arnold Rev.Sci Instrum. 1991, **62**, 3025.
21 E.J. Davis, M.F. Buehler, and T.L.Ward, *Rev.Sci.Instrum* 1990, **61**, 1281.
22 R.A. Shaw, D.Lamb, and A.M.Moyle, *J. Atmos. Oceanic Technol.* 2000, 17, 940.
23 E.E.Allison and B.R.F. Kendall, *Rev.Sci.Instrum.* 1996, 67, 3806.
24 M.Itoh, E. Arakawa, K. Sakiyama, K.Tanaka, K. and H. Takano, J.Aerosol Sci. 1999, **30**, S403.
25 H. Ulmke, T. Wriedt, and K. Bauckhage, Chem. Eng. Technol. 2001, **24**, 265; E.R. Lee and M.L. Perl, 1999, U.S. Pat. No. 5943075.
26 S. Dehaeck, S. and J.P.A.J van Beeck, *Exp. Fluids* 2008, **45** , 823.
27 M. Zientara, D. Jakubczyk, G. Derkachov, K.Kolwas, K. and M. Kolwas, *J.Phys. D*, 2005, **38**, 1978.
28 H. El-Kashef, *Physica B* 2000, **279**, 295.
29 E.A.Mason and S.C. Saxena *Phys. Fluids* 1958, **1**, 361; R.A. Perkins, H.M. Roder, D.G. Friend, C.A. Nieto de Castro, *Physica A* 1991, **173**, 332.
30 S. Chapman and T.G. Cowling, *The Mathematical Theory of Non-Uniform Gases* 1990 (Cambridge University Press)
31 S. Jennings, Journal of Aerosol Science 1988, **19**, 159.
32 F. Muller-Plathe, *J. Chem. Phys*. 1997, **106**, 6082.

View Article Online
DOI: 10.1039/C3SM50997D

33 D. Jakubczyk, M.Kolwas, G. Derkachov, K. Kolwas, and M. Zientara , *Acta Physica Polonica A* 2012, **122**, 709.
34 M.Zientara, D. Jakubczyk, K. Kolwas and M. Kolwas, *J. Phys. Chem. A* 2008, **112**, 5152.
35 R.Holyst and M.Litniewski, *J.Chem.Phys*. 2009, **130**, 074707.
36 M.Zientara, D.Jakubczyk, M.Litniewski and R.Holyst, *J.Phys.Chem. C* 2013, **117**, 1146.